DINAME 2017 - Proceedings of the XVII International Symposium on Dynamic Problems of Mechanics
A. T. Fleury, D. A. Rade, P. R. G. Kurka (Editors), ABCM, São Sebastião, SP, Brazil, March 5-10, 2017

Analysis of the Dynamic Behavior of a Cracked Rotating Shaft by Using the Harmonic Balance Approach

Aldemir Ap Cavalini Jr[1], Tobias Souza Morais[1], Nicolò Bachschmid[2], Valder Steffen Jr[1]

[1] LMEst – Structural Mechanics Laboratory, Federal University of Uberlândia, School of Mechanical Engineering, Av. João Naves de Ávila, 2121, Uberlândia, MG, 38408-196, Brazil, aacjunior@ufu.br, tobias@ufu.br, vsteffen@ufu.br.

[2] Department of Mechanical Engineering, Politecnico di Milano, Via La Masa 1, Milano, 20156, Italy, nicolo.bachschmid@polimi.it.

Abstract: There are several SHM techniques proposed in the literature for crack detection in rotating machines. Among them, the ones based on vibration measurements are recognized as useful tools in the industrial context. Although widely used, when applied under non-ideal conditions, such techniques can only detect cracks that eventually have already spread significantly along the cross section of the shaft (usually above 40% of its diameter). Therefore, currently, the researchers' attention is turning to more sophisticated methods capable of identifying incipient cracks (cracks that spread up to 25% of shaft diameter), which represent a type of damage that are hardly observable in classical vibration analysis. In a previous contribution, a crack identification methodology based on a nonlinear approach was proposed. The technique uses external applied diagnostic forces at certain frequencies attaining combinational resonances, together with a pseudo-random optimization code, known as Differential Evolution, in order to characterize the signatures of the crack in the spectral responses of flexible rotor. In the present paper, the favorable conditions to apply the proposed methodology are investigated. The analysis procedure is confined to the operating parameters of the system, being characterized by the rotation speed of the rotor and the amplitude and frequency of the diagnostic forces. The harmonic balance approach is used to determine the vibration responses of the cracked rotor system and the open crack behavior is simulated according to the FLEX model. For illustration purposes, a rotor composed by a horizontal flexible shaft, two rigid discs, and two self-aligning ball bearings is used to compose a FE model of the system.

Keywords: rotordynamics, crack detection and identification, FLEX model, harmonic balance approach.

INTRODUCTION

Shaft crack detection is an important issue in rotor dynamics and machines that are suspect of having a crack must be treated with the upmost concern (Bently and Hatch, 2002). The importance attributed to this problem is addressed to the serious consequences when cracks are not early identified in rotating systems. Thus, manufacturers have adopted design concepts, as well as special procedures for start-up, operation, monitoring, and maintenance, in order to minimize the appearance and growth of cracks in different rotors, such as steam turbines, centrifugal compressors, and generator units found in power plants. Various structural health monitoring (SHM) techniques devoted to crack detection in rotating machines have been proposed in the last decade. Therefore, the methodologies that use harmonic excitations as diagnostic forces has attracted the attention of several researchers and two interesting results are here recalled.

Mani, Quinn, and Kasarda (2006) presented a theoretical analysis considering a simple rotor model with 2 degrees of freedom containing a breathing crack. The method of multiple scales was used to solve the equations of motion of the system, in which the stiffness of the shaft was affected by the nonlinearity (i.e., the breathing crack). The so-called combination vibrations were defined in the context of rotating cracked shafts. It was shown that the vibration amplitudes associated with the combination vibrations are directly proportional to the time dependent stiffness; in other words, to the crack depth. Ishida and Inoue (2006) made accurate numerical and analytical analyzes on a cracked Jeffcott rotor. The stiffness of the cracked shaft has been modeled by using two different approaches, namely, *i)* a piecewise linear stiffness, and *ii)* by using power series. The effects of the excitation intensity (diagnostic forces) on the forward and backward whirl vibration responses of the rotor system at the combination frequencies were evaluated according to the crack severity. An experimental validation of the proposed method was presented, in which the combination vibrations were demonstrated on the vibration responses of the considered rotating machine.

More recently, Cavalini Jr et al. (2016) have analyzed the possibility of identifying the severity of transverse cracks (i.e., position and depth) in rotating shafts by using the so-called diagnostic forces and the combination vibrations. The frequencies of the diagnostic forces were determined by using the method of multiple scales. This model based approach (i.e., considering the finite element model of the system – FE model) was applied in a rotor test rig composed by a horizontal shaft, two rigid discs, two self-alignment ball bearings, and one electromagnetic actuator used to apply the harmonic excitations. The horizontal vibration responses of the rotating machine were measured by using displacement sensors located near to the discs. The dynamic behavior of the system was investigated considering the breathing and open crack models. The crack models were formulated from the Mayes model (breathing crack) allied to the linear fracture mechanics approach (breathing and open cracks). Vibration responses in the time domain have been determined for different crack positions and depths. In a given test case, the proposed methodology was able to identify, with good accuracy, the severity of the crack by using the Differential Evolution optimization method (Storn and Price, 1995). In that contribution constant rotation speed and various diagnostic excitations at frequencies suitable for exciting two combination vibrations were considered.

The purpose of applying the diagnostic forces in a cracked shaft at frequencies Ω_d different from the rotation speed Ω is to exciting combination vibrations. The natural frequency (Ω_n; i.e., forward and backward natural frequencies of the shaft operating at Ω) and rotation speed of the rotor are used to determine the conditions in which the combination vibrations appear, which results in the frequencies of the diagnostic forces (i.e., $\Omega_d = 2\Omega - \Omega_n$, $\Omega_d = -2\Omega + \Omega_n$, $\Omega_d = 4\Omega - \Omega_n$, $\Omega_d = -4\Omega + \Omega_n$, etc - in the case of open crack). Significant vibration amplitudes can be observed at these frequencies, allowing to distinguish the resonance peak from other vibration components and noise. The natural frequencies of the shaft must be known, so that the frequencies of the diagnostic forces can be selected in advance. However, the problem consists in determining the amplitude and frequency of the diagnostic forces to generate measurable peaks on the vibration spectrum at the combination vibrations. This is an important issue, mainly when the proposed technique is applied in industrial machinery due to the limitations regarding the applicable force amplitude and position.

Therefore, the vibration response of the system at the combination vibrations depends on the damping, the location of the crack in the shaft, the locations where the diagnostic forces are applied, and the amplitude of the diagnostic forces. In this paper, the dynamic behavior of a cracked rotating shaft is analyzed to determine the most favorable conditions to apply the mentioned SHM technique by using the harmonic balance approach. This quasi-linear methodology is able to determine the vibration amplitudes at the combination vibrations generated by the presence of the crack when the external diagnostic forces are applied in the rotor system. Additionally, the obtained results are compared to the ones determined from the trapezoidal rule integration scheme, which was coupled with the Newton-Raphson iterative method for nonlinear analysis (Cavalini Jr et al., 2015).

It is worth mentioning that cracks may be always open or they can breathe depending on the rotating machine and operating conditions. Shafts affected by open cracks behave according to linear systems with parametric excitation. Differently, shafts with breathing cracks becomes really non-linear when dominated by vibrations. It may occur in vertical shafts or in horizontal light and weakly damped shafts. However, shafts with breathing cracks may also be considered linear systems when the dynamic behavior is weight dominated, as occurs in horizontal rotating heavy shafts. In this contribution, the study is restricted to linear systems with parametric excitation. Thus, the so-called FLEX model for open cracks is used (Bachschmid, Pennacchi, and Tanzi, 2010).

ROTOR TEST RIG

Figure 1a shows the rotor test rig used to represent the analyzed rotor system, leading to the numerical simulations shown in this work. Thus, a model with 33 finite elements (Timoshenko's beam elements with 4 degrees of freedom per node; Fig. 1b) was used to mathematically characterize the system. It is composed of a flexible steel shaft with 860 mm length and 17 mm diameter (E = 205 GPa, ρ = 7850 kg/m^3, υ = 0.29), two rigid discs D_1 (node #13; 2.637 kg; according to the FE model) and D_2 (node #23; 2.649 kg), both of steel and with 150 mm diameter and 20 mm thickness (ρ = 7850 kg/m^3), and two roller bearings (B_1 and B_2, located at nodes #4 and #31, respectively). Displacement sensors are orthogonally mounted at nodes #8 (S_{8X} and S_{8Z}) and #28 (S_{28X} and S_{28Z}) to measure the shaft vibration. The system is driven by an electric DC motor.

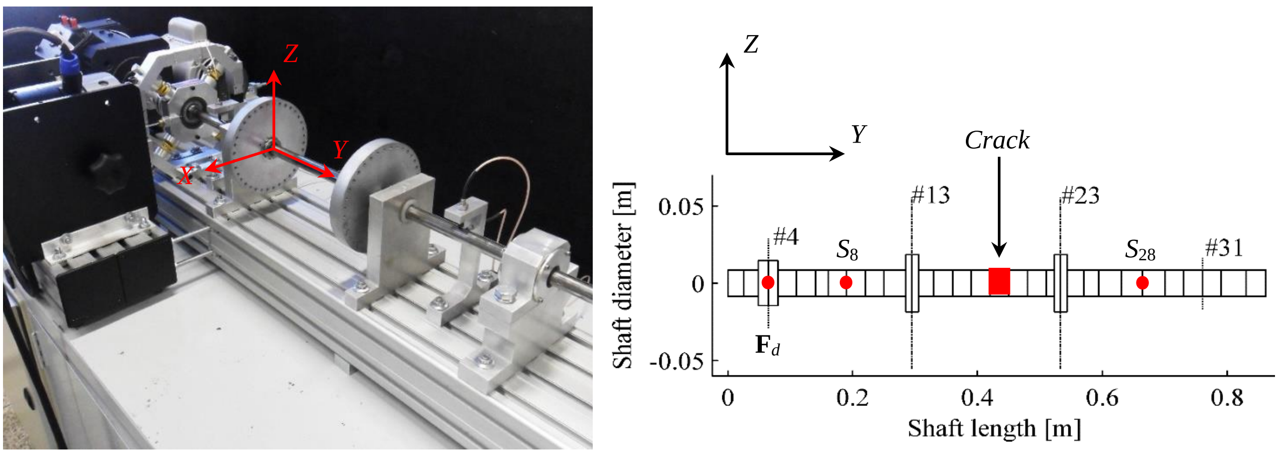

(a) (b)

Figure 1 – Rotor test rig used in the numerical simulations of the SHM technique: a) Test rig; b) FE model.

Equation (1) governs the dynamic behavior of the cracked flexible rotor supported by roller bearings (Lalanne and Ferraris, 1998).

$$\mathbf{M}\ddot{\mathbf{q}} + \left[\mathbf{D} + \Omega \mathbf{D}_g\right]\dot{\mathbf{q}} + \mathbf{K}(\Omega t)\mathbf{q} = \mathbf{W} + \mathbf{F}_u + \mathbf{F}_d \tag{1}$$

where **M** is the mass matrix, **D** is the damping matrix, $\mathbf{D}_g$ is the gyroscopic matrix, and $\mathbf{K}(\Omega t)$ is the periodic stiffness matrix with variable values due to the crack (i.e., Ωt is the angular position of the shaft). **W** stands for the weight of the rotating parts, $\mathbf{F}_u$ represents the rotating unbalance forces, and $\mathbf{F}_{diag}$ represents the diagnostic force applied in the rotor (force fixed in space), and **q** is the generalized displacement vector.

A model updating procedure was used in order to obtain a representative FE model, considering the rotor system in a pristine condition (Fig. 1). In this sense, a heuristic optimization technique (Differential Evolution) was used to determine the unknown parameters of the model, namely the stiffness and damping coefficients of the bearings, the proportional damping added to **D** (coefficients γ and β; $\mathbf{D}_p = \gamma\,\mathbf{M} + \beta\,\mathbf{K}$), and the angular stiffness k_{ROT} due to the coupling between the electric motor and the shaft (added around the orthogonal directions X and Z of the node #1).

The proposed identification process (i.e., the comparison between simulated and experimental frequency response functions, FRF) was performed 10 times, considering 100 individuals in the initial population of the optimizer. However, in this case only the regions close to the peaks associated with the natural frequencies were taken into account. Table 1 summarizes the parameters determined at the end of the minimization process associated with the smaller fitness value (i.e. objective function value). Figure 2 presents the Campbell diagram of the rotating machine, in which the first two forward critical speeds were determined at, approximately, 1714 rev/min and 5912 rev/min. More details about the model updating procedure adopted in this work can be found in Cavalini Jr et al. (2016).

Table 1 – Parameters determined by the model updating procedure.

Parameters	Values	Parameters	Values	Parameters	Values
k_X / B_1	8.551×10^5	k_X / B_2	5.202×10^7	γ	2.730
k_Z / B_1	1.198×10^6	k_Z / B_2	7.023×10^8	β	4.85×10^{-6}
d_X / B_1	7.452	d_X / B_2	25.587	k_{ROT}	770.442
d_Z / B_1	33.679	d_Z / B_2	91.033		

**k*: stiffness [N/m]; *d*: damping [Ns/m].

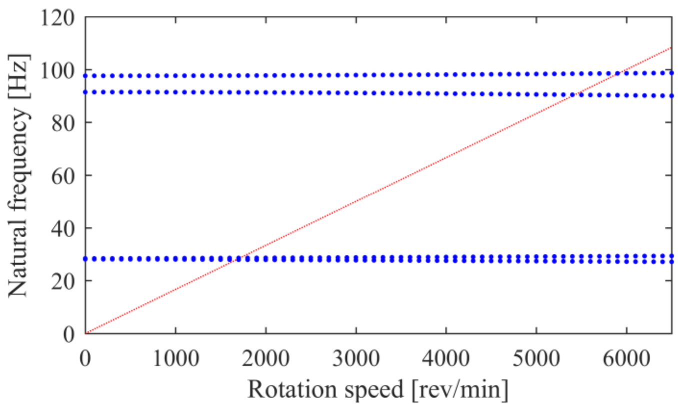

Figure 2 – Campbell diagram of the rotating machine.

OPEN CRACK MODEL

Three models are the most currently used to represent the breathing behavior. The models proposed by R. Gasch (Gash, 1976) and I.W. Mayes and W.G.R. Davies (Mayes and Davies, 1984) are weight dominated. In both, the mechanism for opening and closing the crack is described by simple mathematical functions. The Gasch's model considers the crack as opening and closing abruptly, while the Mayes' model allows a smooth transition between the fully opened and fully closed crack. Finally, there is the more sophisticate model, known as FLEX model, as proposed by Bachschmid, Pennacchi, and Tanzi (2010).

The FLEX model was originally formulated for breathing cracks, in which the dynamic phenomena is characterized by the stress distribution on the crack cross-section (σ_{FLEX}; see Eq. (2)). For a given angular position Ωt of the shaft, the locations of the crack cross-section presenting tensile stresses are considered open. Differently, compressive stresses represent crack closed regions.

$$\sigma_{FLEX} = \frac{M_Z I_{XX} + M_X I_{XZ}}{I_{XX} I_{ZZ} - I_{XZ}^2} X_{cr} - \frac{M_X I_{ZZ} + M_Z I_{XZ}}{I_{XX} I_{ZZ} - I_{XZ}^2} Z_{cr} \tag{2}$$

where I_{XX}, I_{ZZ}, and I_{XZ}, are the area inertia moments related to the geometric center (GC) of the shaft cross-section with crack. X_{cr} and Z_{cr} are the distances obtained along the same cross section along the directions X and Z, respectively, from GC to the position where tension is calculated. M_X and M_Z are the dynamic moments around the X and Z directions, respectively. These moments are given by the strength of materials theory and dependent of the external loads applied to the shaft.

The FLEX model results in a symmetrical 8 *x* 8 stiffness matrix named $\mathbf{K}_{FLEX}$ (see Eq. (3)), which is included in the FE model presented by Fig. 1b and Eq. (1) to evaluate the dynamic behavior of the cracked rotor system.

$$\mathbf{K}_{FLEX} = \begin{bmatrix} b_F & p_F & -q_F & -d_F & -b_F & -p_F & -q_F & -d_F \\ & a_F & c_F & q_F & -p_F & -a_F & c_F & q_F \\ & & e_F & r_F & q_F & -c_F & f_F & s_F \\ & & & h_F & d_F & -q_F & s_F & g_F \\ & & & & b_F & p_F & q_F & d_F \\ & & & & & a_F & -c_F & -q_F \\ & & & & & & e_F & r_F \\ SYM & & & & & & & h_F \end{bmatrix} \tag{3}$$

in which,

$$a_F = \frac{12EI_{ZZ}}{L_{FLEX}^3\left(1+\vartheta_{FZZ}\right)} \quad d_F = \frac{6EI_{XX}}{L_{FLEX}^2\left(1+\vartheta_{FXX}\right)} \quad g_F = \frac{EI_{XX}\left(2-\vartheta_{FXX}\right)}{L_{FLEX}\left(1+\vartheta_{FXX}\right)} \quad q_F = \frac{6EI_{XZ}}{L_{FLEX}^2\left(1+\vartheta_{FXZ}\right)} \quad \vartheta_{FXX} = \frac{12EI_{XX}}{GSL_{FLEX}^2}$$

$$b_F = \frac{12EI_{XX}}{L_{FLEX}^3\left(1+\vartheta_{FXX}\right)} \quad e_F = \frac{EI_{ZZ}\left(4+\vartheta_{FZZ}\right)}{L_{FLEX}\left(1+\vartheta_{FZZ}\right)} \quad h_F = \frac{EI_{XX}\left(4+\vartheta_{FXX}\right)}{L_{FLEX}\left(1+\vartheta_{FXX}\right)} \quad r_F = \frac{EI_{XZ}\left(4+\vartheta_{FXZ}\right)}{L_{FLEX}\left(1+\vartheta_{FXZ}\right)} \quad \vartheta_{FZZ} = \frac{12EI_{ZZ}}{GSL_{FLEX}^2} \tag{4}$$

$$c_F = \frac{6EI_{ZZ}}{L_{FLEX}^2\left(1+\vartheta_{FZZ}\right)} \quad f_F = \frac{EI_{ZZ}\left(2-\vartheta_{FZZ}\right)}{L_{FLEX}\left(1+\vartheta_{FZZ}\right)} \quad p_F = \frac{12EI_{XZ}}{L_{FLEX}^3\left(1+\vartheta_{FXZ}\right)} \quad s_F = \frac{EI_{XZ}\left(2-\vartheta_{FXZ}\right)}{L_{FLEX}\left(1+\vartheta_{FXZ}\right)} \quad \vartheta_{FXZ} = \frac{12EI_{XZ}}{GSL_{FLEX}^2}$$

with G being the shear modulus, S is the cross-section area of the shaft, and L_{FLEX} is the length of the element as a function of the crack depth (Bachschmid, Pennacchi, and Tanzi, 2010).

For the breathing crack model, the stiffness matrix $\mathbf{K}_{FLEX}$ is updated according to the applied external loads for each angular position of the shaft. The iterative process is based on the identification of the remaining cracked area cross section, which is given by the stress distribution σ_{FLEX} determined by Eq. (2). Thus, the area moments of inertia presented in Eq. (4) are determined allowing the stiffness matrix calculation of the cracked element. In the open crack model, the stiffness matrix $\mathbf{K}_{FLEX}$ is only dependent of the angular position Ωt and the area moments of inertia can be written as follows:

$$\begin{aligned} I_{XX}(\Omega t) &= \frac{I_{xx}+I_{zz}}{2} + \frac{I_{xx}-I_{zz}}{2}\cos(2\Omega t) \\ I_{ZZ}(\Omega t) &= \frac{I_{xx}+I_{zz}}{2} - \frac{I_{xx}-I_{zz}}{2}\cos(2\Omega t) \\ I_{XZ}(\Omega t) &= -\frac{I_{xx}-I_{zz}}{2}\sin(2\Omega t) \end{aligned} \tag{5}$$

where I_{xx} and I_{zz} are the area moments of inertia of the shaft cross-section with crack about rotating *x*- and *z*-axes as defined by AL-Shudeifat (2013).

As mentioned, the open crack behavior is a function of the shaft angular position Ωt only. Therefore, the periodic stiffness matrix of the shaft $\mathbf{K}(\Omega t)$ (see Eq. (1)) can be written according to Eq. (6).

$$\mathbf{K}(\Omega t) = \mathbf{K}_m + \sum_{j=1}^{3}\frac{1}{2}\left(\Delta\mathbf{K}_j\, e^{i j\Omega t} + \Delta\mathbf{K}_j^*\, e^{-i j\Omega t}\right) \tag{6}$$

where $\mathbf{K}_m$ is the mean stiffness matrix of the shaft with the crack and $\Delta\mathbf{K}_j$ (j = 1, 2, and 3) are the stiffness variation related to the 1X, 2X, and 3X vibration components of the rotor speed. $\Delta\mathbf{K}^*_j$ is the complex conjugate of $\Delta\mathbf{K}_j$. The Fourier expansion of the periodic stiffness is truncated at the third harmonic component. Figure 3 shows the behavior of the stiffness terms described in Eq. (6) considering a 50% depth open crack located at the element #18 of the FE model (see Fig. 1b). Note that the open crack behavior is represented only by the mean stiffness matrix and the component $\Delta\mathbf{K}_2$, which is in accordance with the area inertia moments of Eq. (5).

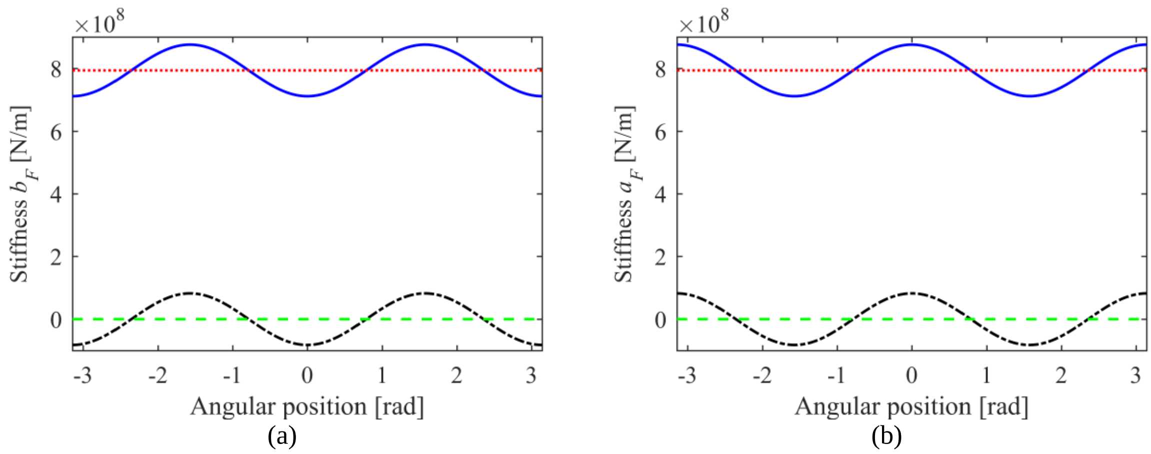

Figure 3 – Stiffness behavior in fixed coordinates (—— K(Ωt); - - - K$_m$; -- -- ΔK$_1$; -- - -- ΔK$_2$; -- -- ΔK$_3$): a) stiffness coefficient b_F; b) stiffness coefficient a_F (see Eq. (3)).

HARMONIC BALANCE APPROCH

As a result of the described open crack model, the equation of motion that governs the dynamic behavior of the flexible rotor can be rewritten as follows:

$$\mathbf{M}\ddot{\mathbf{q}} + \left[\mathbf{D} + \Omega\mathbf{D}_g\right]\dot{\mathbf{q}} + \mathbf{K}_m\mathbf{q} = \mathbf{W} + \mathbf{F}_u + \mathbf{F}_d - \frac{1}{2}\left(\Delta\mathbf{K}_2\,\mathrm{e}^{i2\Omega t} + \Delta\mathbf{K}_2^*\,\mathrm{e}^{-i2\Omega t}\right)\mathbf{q} \tag{7}$$

in which, the vector of degrees of freedom **q** can be expressed as a Fourier series, as shows Eq. (8).

$$\mathbf{q} = \mathbf{q}_{st} + \frac{1}{2}\left(\mathbf{q}_d\,\mathrm{e}^{i\Omega_d t} + \mathbf{q}_d^*\,\mathrm{e}^{-i\Omega_d t}\right) + \frac{1}{2}\left(\mathbf{q}_1\,\mathrm{e}^{i\Omega t} + \mathbf{q}_1^*\,\mathrm{e}^{-i\Omega t}\right) \tag{8}$$

where $\mathbf{q}_{st}$ is the static displacement, $\mathbf{q}_j$ ($j = d$ and 1) are the dynamic displacements related to the diagnostic force and 1X vibration components of the rotor speed due to the unbalance ($\mathbf{q}^*_j$ is the complex conjugate of $\mathbf{q}_j$).

Equation 8 is included in Eq. (7), resulting in new vibration components (i.e., from the last RHS term in Eq. (7)). Therefore, the vector of degrees of freedom must be updated as follows:

$$\begin{aligned}\mathbf{q} = \mathbf{q}_{st} &+ \frac{1}{2}\left(\mathbf{q}_d\,\mathrm{e}^{i\Omega_d t} + \mathbf{q}_d^*\,\mathrm{e}^{-i\Omega_d t}\right) + \frac{1}{2}\left(\mathbf{q}_1\,\mathrm{e}^{i\Omega t} + \mathbf{q}_1^*\,\mathrm{e}^{-i\Omega t}\right) + \frac{1}{2}\left(\mathbf{q}_2\,\mathrm{e}^{i2\Omega t} + \mathbf{q}_2^*\,\mathrm{e}^{-i2\Omega t}\right) + \frac{1}{2}\left(\mathbf{q}_3\,\mathrm{e}^{i3\Omega t} + \mathbf{q}_3^*\,\mathrm{e}^{-i3\Omega t}\right) + \\ &+ \frac{1}{2}\left(\mathbf{q}_{2\Omega+\Omega_d}\,\mathrm{e}^{i(2\Omega+\Omega_d)t} + \mathbf{q}^*_{(2\Omega+\Omega_d)}\,\mathrm{e}^{-i(2\Omega+\Omega_d)t}\right) + \frac{1}{2}\left(\mathbf{q}_{2\Omega-\Omega_d}\,\mathrm{e}^{i(2\Omega-\Omega_d)t} + \mathbf{q}^*_{(2\Omega-\Omega_d)}\,\mathrm{e}^{-i(2\Omega-\Omega_d)t}\right)\end{aligned} \tag{9}$$

where the two last terms of Eq. (9) are the so-called combination vibrations. The resonant condition is induced in the cracked rotating shaft when one of the combination frequencies equals one of the critical speeds (i.e., $\Omega_c = 2\Omega + \Omega_d$ and $\Omega_c = 2\Omega - \Omega_d$). The substitution process continues including Eq. (9) in Eq. (7). Different vibration components and combination vibrations are determined.

Equation 10 presents the amplitudes of the equivalent forces $\mathbf{F}_j$ associated with the vibration components 0, Ω_d, Ω, 2Ω, 3Ω, and 4Ω, and the combination vibrations $2\Omega + \Omega_d$, $2\Omega - \Omega_d$, $4\Omega + \Omega_d$, $4\Omega - \Omega_d$, $6\Omega + \Omega_d$, and $6\Omega - \Omega_d$ ($j = st$, Ω_d, 1, 2, …, $6\Omega + \Omega_d$, and $6\Omega - \Omega_d$). The forces were obtained from subsequent substitutions of the vector of degrees of freedom in the last RHS term of Eq. (7). Note that the forces at Ω and 3Ω ($\mathbf{F}_1$ and $\mathbf{F}_3$, respectively) are obtained from $\mathbf{q}_1$, $\mathbf{q}_3$, $\mathbf{q}^*_1$, and $\mathbf{q}_5$; i.e., odd vibration components. Differently, $\mathbf{F}_{st}$, $\mathbf{F}_2$, and $\mathbf{F}_4$ are proportional to even vibration components and $\mathbf{q}_{st}$. Additionally, the equivalent forces at the combinations resonances depend on the frequency of the diagnostic force Ω_d and the even vibration components 2Ω, 4Ω, 6Ω, and 8Ω. Similar behavior is observed considering the amplitudes at $-\Omega_d$, $-\Omega$, -2Ω, -3Ω, -4Ω, $-(2\Omega + \Omega_d)$, $-(2\Omega - \Omega_d)$, $-(4\Omega + \Omega_d)$, $-(4\Omega - \Omega_d)$, $-(6\Omega + \Omega_d)$, and $-(6\Omega - \Omega_d)$. Therefore, the odd vibration components, as well as the unbalance excitation ($\mathbf{F}_u$ in Eq. (7)), can be disregarded in the analysis of combination vibrations induced in rotating shafts affected by open cracks. Figure 4 presents the vibration responses of the cracked rotating shaft (see Fig. 1b; 50% depth crack located at the element #18) determined by using the trapezoidal rule integration scheme. In this case, two unbalance forces are applied separately to the disc D_1. The diagnostic force was applied along the X direction at the node #4 of the FE model ($\Omega_d = 2\Omega - \Omega_n = 40 – 28.5 = 11.5$ Hz; amplitude of 25 N). Note that only the vibration amplitudes at Ω and 3Ω changed according to the unbalance levels, as previously announced.

The equation of motion (see Eq. (7)) can be rewritten in a matrix form, according to the considered vibration components and combination vibrations. Equation 11 presents the problem formulated to determine the vibration responses of the cracked rotating shaft, in which $\mathbf{H}_j$ ($j = d$, 2Ω, 4Ω, 6Ω, …, $2\Omega + \Omega_d$, $2\Omega - \Omega_d$, $4\Omega + \Omega_d$, $4\Omega - \Omega_d$, etc.) is given by Eq. (12) ($\mathbf{H}^*_j$ is the complex conjugate of $\mathbf{H}_j$).

$$\begin{aligned}
&\mathbf{F}_{st} = \frac{1}{4}\Delta\mathbf{K}_2\mathbf{q}_2^* + \frac{1}{4}\Delta\mathbf{K}_2^*\mathbf{q}_2 && \mathbf{F}_{2\Omega+\Omega_d} = \left(\frac{1}{4}\Delta\mathbf{K}_2\mathbf{q}_d + \frac{1}{4}\Delta\mathbf{K}_2^*\mathbf{q}_{4\Omega+\Omega_d}\right)e^{i(2\Omega+\Omega_d)t} \\
&\mathbf{F}_d = \left(\frac{1}{4}\Delta\mathbf{K}_2\mathbf{q}_{2\Omega-\Omega_d}^* + \frac{1}{4}\Delta\mathbf{K}_2^*\mathbf{q}_{2\Omega+\Omega_d}\right)e^{i\Omega_d t} && \mathbf{F}_{2\Omega-\Omega_d} = \left(\frac{1}{4}\Delta\mathbf{K}_2\mathbf{q}_d^* + \frac{1}{4}\Delta\mathbf{K}_2^*\mathbf{q}_{4\Omega-\Omega_d}\right)e^{i(2\Omega-\Omega_d)t} \\
&\mathbf{F}_1 = \left(\frac{1}{4}\Delta\mathbf{K}_2\mathbf{q}_1^* + \frac{1}{4}\Delta\mathbf{K}_2^*\mathbf{q}_3\right)e^{i\Omega t} && \mathbf{F}_{4\Omega+\Omega_d} = \left(\frac{1}{4}\Delta\mathbf{K}_2\mathbf{q}_{2\Omega+\Omega_d} + \frac{1}{4}\Delta\mathbf{K}_2^*\mathbf{q}_{6\Omega+\Omega_d}\right)e^{i(4\Omega+\Omega_d)t} \\
&\mathbf{F}_2 = \left(\frac{1}{2}\Delta\mathbf{K}_2\mathbf{q}_{st} + \frac{1}{4}\Delta\mathbf{K}_2^*\mathbf{q}_4\right)e^{i2\Omega t} && \mathbf{F}_{4\Omega-\Omega_d} = \left(\frac{1}{4}\Delta\mathbf{K}_2\mathbf{q}_{2\Omega-\Omega_d} + \frac{1}{4}\Delta\mathbf{K}_2^*\mathbf{q}_{6\Omega-\Omega_d}\right)e^{i(4\Omega-\Omega_d)t} \\
&\mathbf{F}_3 = \left(\frac{1}{4}\Delta\mathbf{K}_2\mathbf{q}_1 + \frac{1}{4}\Delta\mathbf{K}_2^*\mathbf{q}_5\right)e^{i3\Omega t} && \mathbf{F}_{6\Omega+\Omega_d} = \left(\frac{1}{4}\Delta\mathbf{K}_2\mathbf{q}_{4\Omega+\Omega_d} + \frac{1}{4}\Delta\mathbf{K}_2^*\mathbf{q}_{8\Omega+\Omega_d}\right)e^{i(6\Omega+\Omega_d)t} \\
&\mathbf{F}_4 = \left(\frac{1}{4}\Delta\mathbf{K}_2\mathbf{q}_2 + \frac{1}{4}\Delta\mathbf{K}_2^*\mathbf{q}_6\right)e^{i4\Omega t} && \mathbf{F}_{6\Omega-\Omega_d} = \left(\frac{1}{4}\Delta\mathbf{K}_2\mathbf{q}_{4\Omega-\Omega_d} + \frac{1}{4}\Delta\mathbf{K}_2^*\mathbf{q}_{8\Omega-\Omega_d}\right)e^{i(6\Omega-\Omega_d)t}
\end{aligned} \tag{10}$$

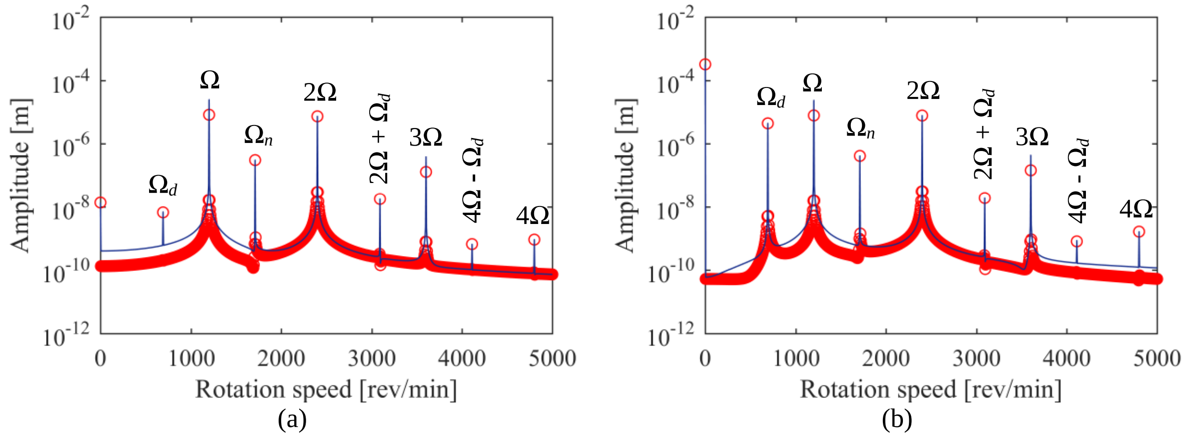

Figure 4 – Vibration responses of the rotating shaft operating at 1200 rev/min (○ 100 g.mm / 0º; —— 300 g.mm / 0º): a) *S*28*X*; b) *S*28*Z*.

$$\begin{bmatrix}
\mathbf{K}_m & \mathbf{0} & \mathbf{0} & \frac{1}{4}\Delta\mathbf{K}_2^* & \frac{1}{4}\Delta\mathbf{K}_2 & \cdots & \mathbf{0} & \mathbf{0} & \cdots \\
\mathbf{0} & \mathbf{H}_d & \mathbf{0} & \mathbf{0} & \mathbf{0} & \cdots & \frac{1}{4}\Delta\mathbf{K}_2^* & \mathbf{0} & \cdots \\
\mathbf{0} & \mathbf{0} & \mathbf{H}_d^* & \mathbf{0} & \mathbf{0} & \cdots & \mathbf{0} & \frac{1}{4}\Delta\mathbf{K}_2 & \cdots \\
\frac{1}{2}\Delta\mathbf{K}_2 & \mathbf{0} & \mathbf{0} & \mathbf{H}_2 & \mathbf{0} & \cdots & \mathbf{0} & \mathbf{0} & \cdots \\
\frac{1}{2}\Delta\mathbf{K}_2^* & \mathbf{0} & \mathbf{0} & \mathbf{0} & \mathbf{H}_2^* & \cdots & \mathbf{0} & \mathbf{0} & \cdots \\
\vdots & \vdots & \vdots & \vdots & \vdots & \ddots & \vdots & \vdots & \cdots \\
\mathbf{0} & \frac{1}{4}\Delta\mathbf{K}_2 & \mathbf{0} & \mathbf{0} & \mathbf{0} & \cdots & \mathbf{H}_{2\Omega+\Omega_d} & \mathbf{0} & \cdots \\
\mathbf{0} & \mathbf{0} & \frac{1}{4}\Delta\mathbf{K}_2^* & \mathbf{0} & \mathbf{0} & \cdots & \mathbf{0} & \mathbf{H}_{2\Omega+\Omega_d}^* & \cdots \\
\vdots & \vdots & \vdots & \vdots & \vdots & \vdots & \vdots & \vdots & \ddots
\end{bmatrix}
\begin{Bmatrix}
\mathbf{q}_{st} \\ \mathbf{q}_d \\ \mathbf{q}_d^* \\ \mathbf{q}_2 \\ \mathbf{q}_2^* \\ \vdots \\ \mathbf{q}_{2\Omega+\Omega_d} \\ \mathbf{q}_{2\Omega+\Omega_d}^* \\ \vdots
\end{Bmatrix}
=
\begin{Bmatrix}
\mathbf{W} \\ \frac{1}{2}\mathbf{F}_{1d} \\ \frac{1}{2}\mathbf{F}_{1d} \\ 0 \\ 0 \\ \vdots \\ \mathbf{0} \\ \mathbf{0} \\ \vdots
\end{Bmatrix} \tag{11}$$

$$\mathbf{H}_j = -\frac{j^2}{2}\mathbf{M} + i\frac{j}{2}\left[\mathbf{D} + \Omega\mathbf{D}_g\right] + \frac{1}{2}\mathbf{K}_m \tag{12}$$

The diagnostic force $\mathbf{F}_d$ is also expressed as a Fourier series. Thus,

$$\mathbf{F}_d = \mathbf{F}_{1d} \cos(\Omega_d t) = \frac{1}{2} \mathbf{F}_{1d} \left(e^{i\Omega_d t} + e^{-i\Omega_d t} \right) \tag{13}$$

where $\mathbf{F}_{1d}$ is the amplitude of the diagnostic force.

NUMERICAL RESULTS

Figure 5 compares the vibration responses of the rotating machine (measuring plane S_{28}) determined by using the harmonic balance approach and the trapezoidal rule integration scheme. This analysis was performed for the rotor under two different structural conditions. The first one comprises the shaft with a crack located at the element #18 with 25% depth. The second test was performed for the shaft with a crack located at the same element with 50% depth. The operational rotation speed of the rotor Ω was fixed to 1200 rev/min and the unbalance forces were disregarded in these results. The diagnostic force was applied along the X direction in the node #4 of the FE model ($\Omega_d = 2\Omega - \Omega_n$ = (40 – 28.5) Hz = 11.5 Hz = 690 rev/min, and amplitude of 25 N). Note that the obtained vibration responses are very close, thus validating the formulation based on the harmonic balance approach. The responses determined along the plane S_8 are similar to the previous ones. It is worth mentioning that vector of degrees of freedom used in this work encompasses the following vibration components: $\mathbf{q}_{st}$, $\mathbf{q}_{\Omega d}$, $\mathbf{q}_{2\Omega}$, $\mathbf{q}_{4\Omega}$, …, $\mathbf{q}_{10\Omega}$, $\mathbf{q}_{2\Omega+\Omega d}$, $\mathbf{q}_{2\Omega-\Omega d}$, $\mathbf{q}_{4\Omega+\Omega d}$, $\mathbf{q}_{4\Omega-\Omega d}$, …, $\mathbf{q}_{10\Omega+\Omega d}$, $\mathbf{q}_{10\Omega-\Omega d}$ (see Eq. (11)).

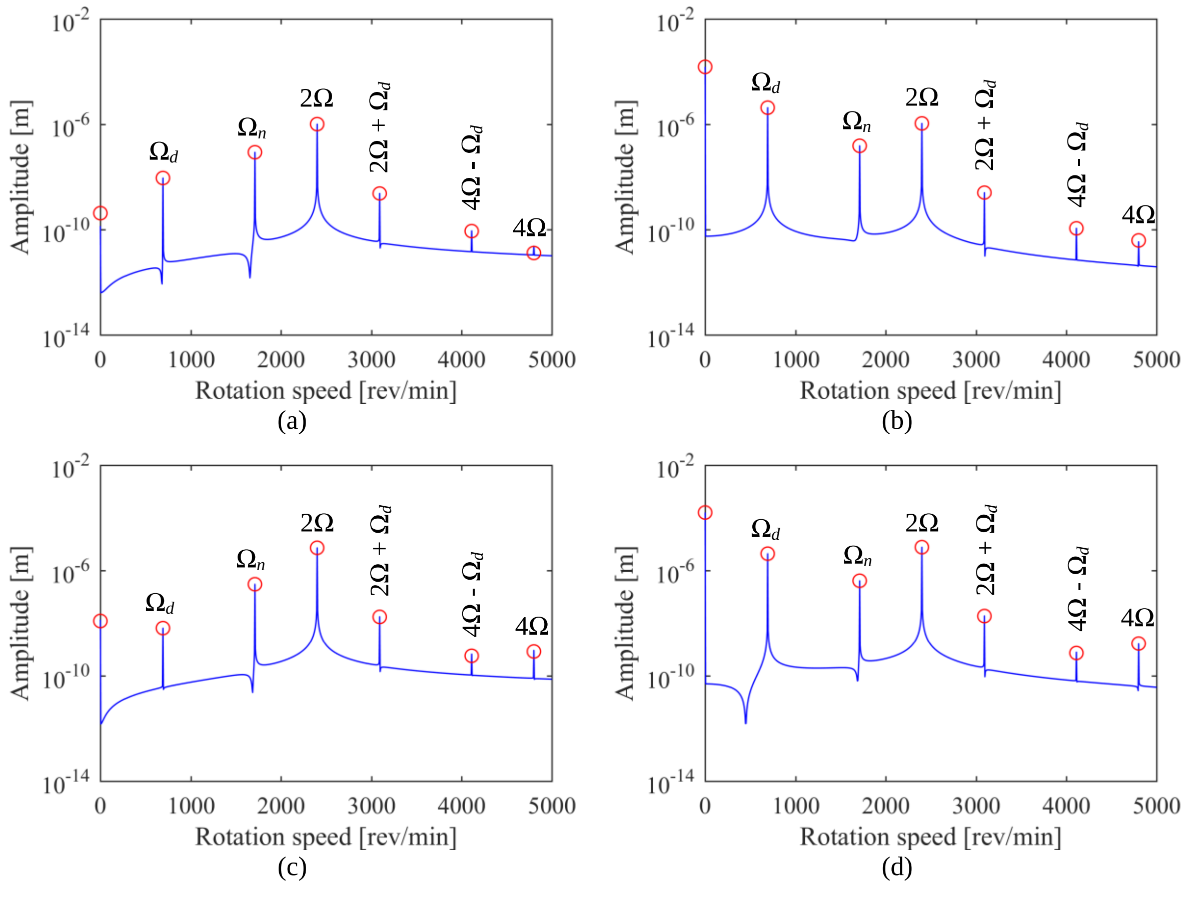

Figure 5 – Vibration responses of the cracked rotating shaft (—— time integration; O harmonic balance): a) 25% crack depth / S_{28x}; b) 25% crack depth / S_{28Z}; c) 50% crack depth /S_{28x}; d) 50% crack depth / S_{28Z}.

Figures 4 and 5 show that the amplitudes at the combination vibrations are too small (< 1.0 μm), affecting the applicability of the considered dynamic phenomenon in crack detection or identification techniques (Sawicki, Storozhev, and Lekki, 2011; Cavalini Jr et al., 2016). As mentioned, the problem consists in determining the amplitude and frequency of the diagnostic forces to generate measurable peaks along the vibration spectrum at the combination vibrations.

Figure 6 presents the vibration responses of the rotor obtained by the sensor S_{28Z} at the frequencies 2Ω + Ω_d, 2Ω - Ω_d, 4Ω + Ω_d, 4Ω - Ω_d, 6Ω + Ω_d, and 6Ω - Ω_d, varying Ω_d from 0 to 85 Hz in steps of 0.1 Hz. The diagnostic forces were applied along the X direction in the node #4 of the FE model with 25 N, 50 N, and 100 N of amplitude, separately. These tests were performed for the shaft with a crack located at the element #18 with 50% depth. The operational rotation speed of the rotor Ω was fixed to 1200 rev/min. No unbalance forces are being considered. Note that measurable peaks (> 1.0 μm) are obtained only at the combinations 2Ω + Ω_d and 2Ω - Ω_d (Fig. 6a and Fig. 6b, respectively). Small vibration amplitudes were obtained for the higher combination frequencies (i.e., 8Ω + Ω_d, 8Ω - Ω_d, 10Ω + Ω_d, 10Ω - Ω_d, etc.). Similar results were observed for the remaining sensors.

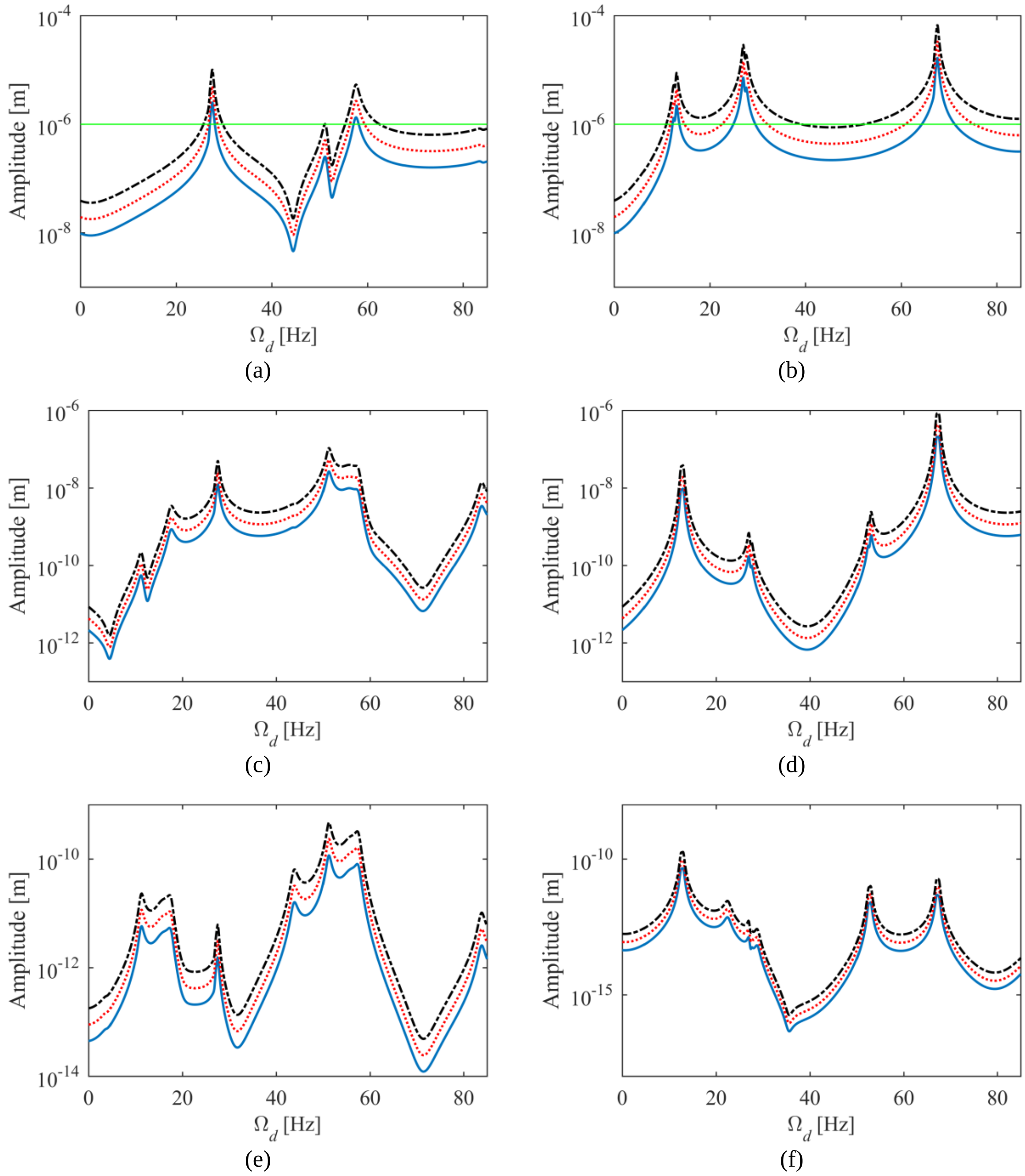

Figure 6 – Vibration responses obtained by the sensor S_{28Z} at the combination vibrations according to Ω_d (—— F_{1d} = 25 N; - - - F_{1d} = 50 N; -- - -- F_{1d} = 100 N): a) 2Ω+Ω_d; b) 2Ω - Ω_d; c) 4Ω+Ω_d; d) 4Ω - Ω_d; e) 6Ω+Ω_d; f) 6Ω - Ω_d.

Figure 6a shows highest vibration amplitudes at 27.5 Hz and 57.6 Hz. In Fig. 6b, significant vibration responses are observed at 13.0 Hz, 27.0 Hz, and 67.5 Hz. It is worth mentioning that the first five natural frequencies of the cracked rotor operating at 1200 rev/min are given by (frequencies in Hz): $26.46 \leq \Omega_{1n} \leq 26.71$, $27.85 \leq \Omega_{2n} \leq 28.14$, $91.03 \leq \Omega_{3n} \leq 91.34$, $97.43 \leq \Omega_{4n} \leq 97.62$, and $123.76 \leq \Omega_{5n} \leq 123.84$ (variation according to the angular position of the shaft). A resonance condition is obtained for Ω_d = 27.5 Hz (frequency close to Ω_{1n} and Ω_{2n}), as well as for Ω_d = 27.0 Hz. Differently, combination vibrations are observed at Ω_d = 57.6 Hz ~ 2Ω + Ω_{2n}, Ω_d = 13.0 Hz ~ 2Ω - Ω_{1n}, and Ω_d = 67.5 Hz ~ 2Ω + Ω_{2n}. Figure 7 presents the vibration responses of the rotor obtained by the sensor S_{28X}. The highest vibration amplitudes are obtained at 27.5 Hz, 51.2 Hz, 83.7 Hz (see Fig. 7a), 13.0 Hz, 27.0 Hz, and 67.6 Hz (see Fig. 7b). Note that along the *X* direction, new combination vibrations are observed at Ω_d = 51.2 Hz ~ Ω_{3n} - 2Ω and Ω_d = 83.7 Hz ~ Ω_{5n} - 4Ω.

CONCLUSIONS

The presented results validate a promising methodology of fault detection, based on the application of a diagnostic force to detect cracks in rotating machines, coupled with a quasi-linear harmonic balancing methodology. This approach exhibits considerable computational time saving as compared with a pure integration in time; besides, it promotes better understanding about the components of the forces acting on the rotating system. Considering the case of a shaft with an

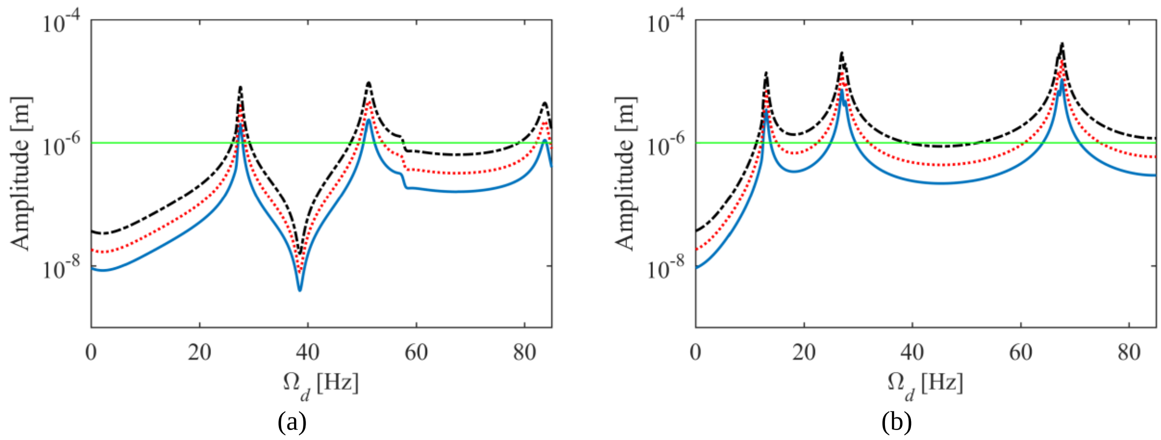

Figure 7 – Vibration responses obtained by the sensor S_{28X} at the combination vibrations according to Ω_d (— F_{1d} = 25 N; - - - F_{1d} = 50 N; -- - -- F_{1d} = 100 N): a) $2\Omega+\Omega_d$; b) $2\Omega - \Omega_d$.

open crack, it was demonstrated that the observed effect on the combination vibrations is just due to the even vibration components. Consequently, in the present case, the odd vibration components, as well as the unbalance influence have been neglected in the analysis. When it was produced a sweep of the diagnostic force frequency, it was observed the combinations $2\Omega + \Omega_d$ and $2\Omega - \Omega_d$ produced the highest measurable peaks exciting the critical speeds below 85 Hz. Finally, the evaluation of the diagnostic force level showed important contribution on the combination vibration emerging. Although, when applied to structure under operating conditions, the amplitude of the diagnostic forces must be regulated to keep the system functioning safely on an acceptable vibration level. The potential of the conveyed techniques will be explored in future research work using combination vibrations.

ACKNOWLEDGMENTS

The authors are thankful to the financial support provided to the present research effort, by CNPq (574001/2008-5) and FAPEMIG (TEC-APQ-3076-09 / TEC-APQ-02284-15), through the INCT-EIE.

REFERENCES

Al-Shudeifat, M.A, 2013, On the Finite Element Modeling of the Asymmetric Cracked Rotor, Journal of Sound and Vibration, Vol. 332, No. 11, pp. 2795-2807.

Bachschmid, N., Pennacchi, P., and Tanzi, E., 2010, Cracked Rotors: A Survey on Static and Dynamic Behaviour Including Modelling and Diagnosis, Springer-Verlag, Berlin, Germany.

Bently, D.E. and Hatch, C.T., 2002, Fundamentals of Rotating Machinery Diagnostics, Bently Pressurized Bearing Company, Minden, NV, USA.

Cavalini Jr, A.A., Sanches, L., Bachschmid, N., and Steffen Jr, V., 2016, Crack Identification for Rotating Machines Based on a Nonlinear Approach, Mechanical Systems and Signal Processing, Vol. 1, No. 1, pp. 1-14.

Cavalini Jr, A. A., Lara-Molina, F.A., Sales, T.P., Koroishi, E.H., and Steffen Jr, V., 2015, Uncertainty Analysis of a Flexible Rotor Supported by Fluid Film Bearings, Latin American Journal of Solids and Structures, Vol. 12, No. 8, pp. 1487-1504.

Gasch, R., 1976, Dynamic Behaviour of a Simple Rotor with a Cross Sectional Crack. In: International Conference on Vibrations in Rotating Machinery, IMechE, Vol. 1, No. 1, pp. 123-128.

Ishida, Y. and Inoue, T., 2006, Detection of a Rotor Crack Using a Harmonic Excitation and Nonlinear Vibration Analysis, Journal of Vibration and Acoustics, Vol. 128, No. 1, pp. 741-749.

Lalanne, M. and Ferraris, G., 1998, Rotordynamics Prediction in Engineering, Second Edition, John Wiley and Sons.

Mani, G., Quinn, D.D., and Kasarda, M., 2006, Active Health Monitoring in a Rotating Cracked Shaft using Active Magnetic Bearings as Force Actuators, Journal of Sound and Vibration, Vol. 294, No. 1, pp. 454-465.

Mayes, I.W. and Davies, W.G.R., 1984, Analysis of the Response of a Multi-Rotor-Bearing System Containing a Transverse Crack in a Rotor, Journal of Vibration, Acoustics, Stress, and Reliability in Design, Vol. 106, No. 1, 0 pp. 139-145.

Sawicki, J.T., Storozhev, D.L., and Lekki, J.D., 2011, Exploration of NDE Properties of AMB Supported Rotors for Structural Damage Detection, Journal of Engineering for Gas Turbines and Power, Vol. 133, No. 1, pp. 1-9.

Storn, R. and Price, K., 1995, Differential Evolution - a Simple and Efficient Heuristic for Global Optimization over Continuous Spaces, Journal of Global Optimization, Kluwer Academic Publishers, Vol. 11, No. 1, pp. 341-359.

RESPONSIBILITY NOTICE

The authors are the only responsible for the material included in this paper.